An Optical Reservoir Computing Design based on Two-Dimensional Quantum Walk

1st Yushu Wang
School of Optical and Electronic Information
Huazhong University of Science and Technology
Wuhan, China
wys_anicy@hust.edu.cn

2nd Yuheng Ding
School of Optical and Electronic Information
Huazhong University of Science and Technology
Wuhan, China
u202214727@hust.edu.cn

3rd Yang Chen
School of Optical and Electronic Information
Huazhong University of Science and Technology
Wuhan, China
yang_chenc@hust.edu.cn

4th Yangcan Long
School of Optical and Electronic Information
Huazhong University of Science and Technology
Wuhan, China
yangcanlong@cug.edu.cn

5th Ming Tang
School of Optical and Electronic Information
Huazhong University of Science and Technology
Wuhan, China
tangming@hust.edu.cn

6th Chao Wang
School of Optical and Electronic Information
Huazhong University of Science and Technology
Wuhan, China
chao_wang_me@hust.edu.cn

***Abstract*—Optical computing based on quantum effects has attracted extensive attention over the past decades. Recently, Quantum Extreme Learning Machine (QELM) utilizing quantum walk effect has been explored as an emerging architecture for quantum signal processing. However, the QELM suffers from the absence of complex dynamical behaviors and accurate nonlinear fitting capabilities. To address these challenges, this paper proposes a novel Two-Dimensional Quantum Walk Reservoir Computing (2D-QWRC) model. Evaluation results indicate that the proposed optical reservoir computing design based on the 2D quantum walk effect can reduce the training error in nonlinear function fitting tasks by 26.72% compared to the conventional QELM. Furthermore, the introduction of entanglement effects implemented by Controlled NOT gate contributes to an additional reduction in training error by approximately 37.60%. The effectiveness of 2D-QWRC is also validated with a prediction accuracy of 82% on the Abalone data set recognition task.**

Keywords—optical computing, quantum reservoir computing, quantum walk

I. INTRODUCTION

Reservoir computing (RC) represents a classical non-von Neumann computational paradigm, which leverages the dynamical properties of multiple physical systems to project input data into high-dimensional spaces. Through the RC architecture, classification or prediction tasks can be effectively performed using simple linear regressors [1]. Quantum reservoir computing is a class of emerging RC approaches that harnesses the complex and diverse dynamics of quantum systems. Over the past decades, RC has gradually been implemented across a variety of quantum platforms [2-4]. Notably, quantum photonics has been recently employed in experimental setups to demonstrate quantum computational advantage, and therefore, it becomes a popular platform for implementing quantum reservoir computing [5].

Extreme learning machine is an emerging learning framework similar to reservoir computing, but with simpler internal dynamics and typically without recurrent information propagation [6]. Recently, Quantum Extreme Learning Machine (QELM) based on effects of optical one-dimensional quantum walk has been presented as a quantum information reconstructor [7]. However, QELM system has been proven to have weak non-linearity, because the non-linearity comes solely from encoding process, and the dynamics of one-dimensional quantum walk do not possess non-linearity [8]. The consequent insufficient nonlinear fitting ability has been a significant disadvantage, which constrains its applicability to general machine learning tasks.

In fact, one-dimensional quantum walk can be exactly mapped onto classical wave phenomena, which prevents it from exhibiting complex quantum behaviors such as entanglement and therefore, loses the potential computational advantages introduced by such behaviors [9]. In contrast, two-dimensional quantum walk not only offers richer nonlinear encoding capabilities, but also enables the emergence of intricate dynamical features like quantum entanglement. Therefore, it is very promising to improve the optical computing performance by exploiting the complex dynamical nature of two-dimensional quantum walk for reservoir computing.

In this paper, a novel quantum reservoir computing design based on two-dimensional quantum walk effect is proposed. Compared with computation models utilizing lower-dimensional quantum walk, such as QELM, the proposed design demonstrates notably enhanced nonlinear fitting capability without increasing the weight parameter scale of output layer. Evaluation on both the nonlinear function approximation and prediction tasks using the Abalone data set is carried out. Discussions on the influences of entanglement on the model's performance and the possible optical implementations of each layer are also provided, indicating the feasibility of the proposed optical design as well as future research potentials.

II. PRINCIPLES AND FRAMEWORK

Quantum walk is a quantum phenomenon characterized by one intrinsic degree of freedom within a specific quantum state controlling the walk of another parameter of that state [10]. It is divided into two categories: discrete quantum walk and continuous quantum walk. In a discrete quantum walk,

This work was jointly supported by the Open Project Program of Wuhan National Laboratory for Optoelectronics (2022WNLOKF011) and National Natural Science Foundation of China 62225110. Corresponding author: Chao Wang.

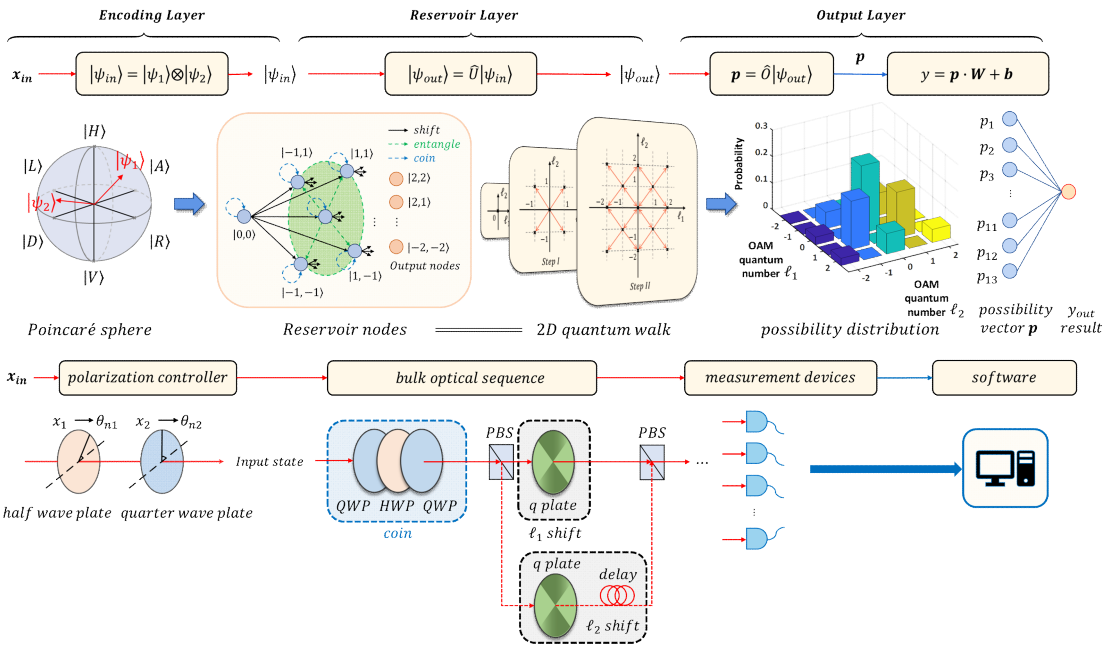

Fig. 1. Schematic diagram of two-dimensional quantum walk reservoir computing principles and implementation methodology.

coin operator and shift operator are applied alternately on the quantum state, i.e., the walker [10]. The coin operator modifies the intrinsic degree of freedom, while the shift operator conditionally shifts the controlled parameter. One full step of the walk includes a coin operator followed by a shift operator.

Fig. 1 presents the framework of Two-Dimensional Quantum Walk Reservoir Computing (2D-QWRC) model consisting of an encoding layer, a reservoir layer, and an output layer. The operational principles of each layer are elaborated in the following subsections.

A. Encoding Layer

In the encoding layer, the input is encoded on polarization states as shown in Fig. 1. A single-photon laser attenuator followed by optical polarization elements [11] or integrated photonic polarization controller [12] can be utilized for the generation of these polarization states. In this study, a sequence of optical elements is modeled, which consists of half-wave plates (HWPs), and quarter-wave plates (QWPs). A two-dimensional quantum walk can be equivalently modeled as two walkers of $|\psi_1\rangle$ and $|\psi_2\rangle$ walking in one-dimensional space. Furthermore, the encoding layer provides a single walker $|\psi_n\rangle$ with two degrees of freedom, i.e., θ_{n1}, θ_{n2}. In practical learning tasks, the input data $\boldsymbol{x}_{in}$ is linearly mapped onto these two parameters, which can be represented as

$$\boldsymbol{x}_{in} = [x_1 \quad x_2 \quad x_3 \quad x_4]^T \tag{1}$$

$$\begin{bmatrix} x_1 \\ x_2 \end{bmatrix} = m \begin{bmatrix} \theta_{11} \\ \theta_{12} \end{bmatrix}, \begin{bmatrix} x_3 \\ x_4 \end{bmatrix} = m \begin{bmatrix} \theta_{21} \\ \theta_{22} \end{bmatrix} \tag{2}$$

where $\boldsymbol{x}_{in}$ stands for the input data in vector form. The mapping coefficients m are tuned to avoid effects of the angular periodicity of waveplates. Thus, the overall input quantum state $|\psi_{in}\rangle$ can be constructed by taking the tensor product of individual walkers' states, as described by

$$|\psi_n\rangle = \frac{1}{\sqrt{2}}\left[e^{i\theta_{n1}}(\cos(2\theta_{n2} - \theta_{n1}) - \sin(2\theta_{n2} - \theta_{n1}))|L\rangle \right.$$
$$\left. + e^{-i\theta_{n1}}(\cos(2\theta_{n2} - \theta_{n1}) + \sin(2\theta_{n2} - \theta_{n1}))|R\rangle \right] \quad (\mathrm{n} = 1,2) \tag{3}$$

$$|\psi_{in}\rangle = |\psi_1\rangle \otimes |\psi_2\rangle \tag{4}$$

where $|L\rangle$ and $|R\rangle$ stand for left- and right-circular polarization, respectively. θ_{n1} and θ_{n2} denote the rotation angles of optical axes of the HWP and QWP of the n^{th} walker, respectively.

B. Reservoir Layer

In the reservoir layer, the total input state $|\psi_{in}\rangle$ undergoes two steps of quantum walk to generate a probability distribution, as shown in Fig. 1.

A variety of physical systems have been used for implementing both continuous and discrete quantum walks, including superconducting qubits, laser beams and bulk optics, and integrated photonics systems [13]. Moreover, optical high-dimensional quantum walk can usually be implemented by bulk optics with time-multiplexing structures [14] or integrated photonics [15].

The bulk optics implementation of discrete two-dimensional quantum walk is considered and modeled in this study, i.e., the combination of q plates, polarization beam splitters (PBSs), QWPs, HWPs and other optical components as illustrated in Fig. 1. The polarization states are utilized as internal degrees of freedom and the controlled walking parameter is orbital angular momentum (OAM) of the propagating beam. Specifically, the coin operator $\hat{C}$ can be implemented using a sequence of waveplates, while the shift operator $\hat{S}$ is realized through q plates with a time-multiplexing system implemented by delay line and two PBSs [16].

For the case of single one-dimensional quantum walk, the coin operators and shift operators can be described by

$$\hat{C} = \begin{pmatrix} e^{-i(\zeta-\phi)}cos\eta & e^{i(\zeta+\phi)}sin\eta \\ -e^{-i(\zeta+\phi)}sin\eta & e^{i(\zeta-\phi)}cos\eta \end{pmatrix} \tag{5}$$

$$\eta = \zeta + \phi - 2\theta \tag{6}$$

$$\hat{S} = \sum_{\ell} \Big\{ \cos\frac{\delta}{2}(|L,\ell\rangle\langle L,\ell| + |R,\ell\rangle\langle R,\ell|) + \sin\frac{\delta}{2}(e^{2i\alpha}|L,\ell\rangle\langle R,\ell+1| + e^{-2i\alpha}|R,\ell\rangle\langle L,\ell-1|) \Big\} \quad (7)$$

where $|L,\ell\rangle$ and $|R,\ell\rangle$ denote left- and right- circular polarization with the azimuthal quantum number of OAM being ℓ. The summation in (7) is performed over the entire space reached by the controlled parameters of the walker. Here, the summation range includes all possible values of OAM at the present step. $\zeta, \phi, \theta, \delta, \alpha$ indicate the rotation angles of optical axes of the HWP, two q plates, and two QWPs in one waveplate sequence, respectively.

For the case of two-dimensional quantum walk realized by two one-dimensional walkers, when the two walkers are separable, the total coin operator is expressed as the tensor product of coin operators acting individually on each walker, as described by

$$\hat{C}_{total} = \hat{C}_1 \otimes \hat{C}_2 \quad (8)$$

In cases where entanglement effects begin to emerge, the two walkers are considered non-separable. To reflect these effects, an entanglement coin operator is additionally right-multiplied with the coin operator [17], as described by

$$\hat{C}_{total} = (\hat{C}_1 \otimes \hat{C}_2)\hat{C}_{entangle} \quad (9)$$

Every shift operator in each step corresponds to the tensor product of one-dimensional quantum walk scenarios.

$$\hat{S}_{total} = \hat{S}_1 \otimes \hat{S}_2 \quad (10)$$

From the construction of coin and shift operators in (5) - (10), the complete dynamic of reservoir layer can be described by

$$|\psi_{out}\rangle = (\hat{S}_{total}\hat{C}_{total}\hat{S}_{total})|\psi_{in}\rangle = \hat{U}|\psi_{in}\rangle \quad (11)$$

It is worth noting that in the nonlinear function approximation and prediction tasks in this study, the Controlled NOT gate (CNOT) [18] is used as the entanglement coin operator to provide the entanglement dynamic feature for improving the reservoir computing performance, which is described by

$$\hat{C}_{entangle} = \hat{C}_{CNOT} = \begin{pmatrix} 1 & 0 & 0 & 0 \\ 0 & 1 & 0 & 0 \\ 0 & 0 & 0 & 1 \\ 0 & 0 & 1 & 0 \end{pmatrix} \quad (12)$$

C. Output Layer

In the output layer, the superposition state from the reservoir layer is first converted into a probability distribution through a series of measurements. The 2D probability distribution is then flattened into a vector $\boldsymbol{p}$ to serve as the input to a single-layer trainable network, as shown in Fig. 1. Subsequently, the single-layer network performs a weighted summation on the input to obtain the final output y. This process can be described by

$$\boldsymbol{p} = \hat{O}|\psi_{out}\rangle \quad (13)$$

$$y = \boldsymbol{p} \cdot \boldsymbol{W} + \boldsymbol{b} \quad (14)$$

where $\hat{O}$ stands for the measurement operator, and $\boldsymbol{p}$ stands for the probability distribution vector of the superposition state $|\psi_{out}\rangle$. $\boldsymbol{W}$ and $\boldsymbol{b}$ denote the weight vector and the bias vector of single layer trainable network, respectively.

In the proposed design, the series of measurements are performed to possess the probability of quantum states with specific OAM values. The measurements are usually carried out by spatial light modulators and avalanche photodiode detectors [16]. The single-layer trainable network is commonly implemented by software in general processors. In this study, measurement processes are implemented through numerical computation, and the output layer is trained by utilizing the Levenberg-Marquardt algorithm in MATLAB.

III. Results and Analysis

To validate the improvement in nonlinearity of the proposed 2D-QWRC compared to QELM, the method has been applied to a complex nonlinear function fitting task with performance characterized through fitting error analysis. Furthermore, to explore its potential in general machine learning applications, an abalone age prediction task using both 2D-QWRC and QELM is performed. The simulations are both performed on MATLAB, and the following subsections are the results.

A. Function fitting task

In function fitting task, the applied objective function is

$$f(x) = \frac{\sin \pi x}{\pi x} e^{-x} + 0.01\xi(-3 \le x < 0) \quad (15)$$

where, ξ denotes Gaussian noise randomly generated within the range [0,1]. x values are used as the complete input to the system, and the models are trained using samples from the target function. To eliminate the influence caused by the number of parameters in the output layer, QELM is set to perform 6 steps of quantum walk and 2D-QWRC to perform 2 steps of quantum walk, ensuring that both have 13 channels for the input of output layer.

As demonstrated in Fig. 2 (a), when the mean squared error (MSE) is used to evaluate fitting performance, the QELM model exhibits a relatively high fitting error of 0.4756. In comparison, the 2D-QWRC model without entanglement effects achieves a lower error of 0.3485. Notably, when entanglement effects are incorporated into the 2D-QWRC model, the fitting error further decreases to 0.1697. This represents a total 64.32% reduction in error compared to the QELM model. These results indicate that the 2D-QWRC model possesses superior nonlinear fitting capabilities relative to the QELM.

Fig. 2 (b) illustrates the fitting details of the three architectures. The results indicate that within the two x range segments of -3 to -2 and -1.5 to 0, the output of the 2D-QWRC with entanglement demonstrates significantly improved adherence to the target function compared to both the non-entanglement 2D-QWRC and QELM models. These findings verify two key contributions of this study: Firstly, the 2D-QWRC exhibits superior nonlinear fitting capability relative to the QELM; Secondly, the introduction of entanglement effects to the 2D-QWRC provides advantages for nonlinear fitting tasks.

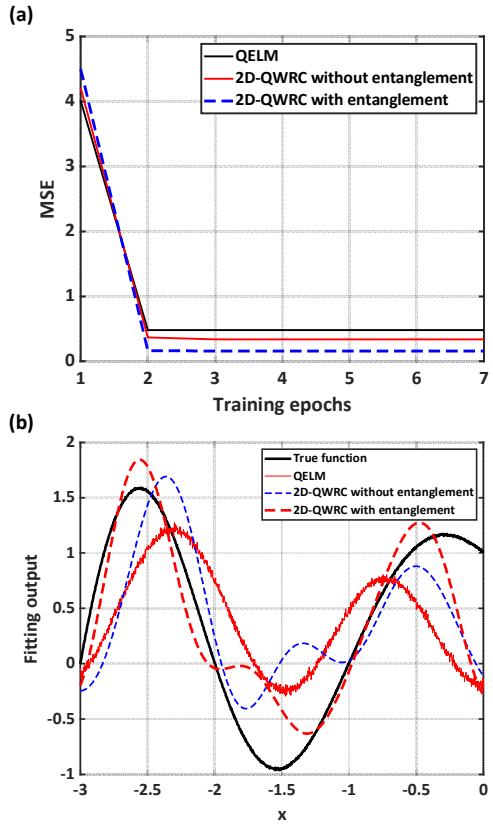

Fig. 2. (a) The variations of MSE with different models during training; (b) The fitting results of different models in nonlinear fitting tasks

To verify whether the advantages introduced by entanglement effects are generalizable, upper triangular matrices and other variants instead of the CNOT matrix in (12) are employed as entanglement coins, yielding the results as shown in Fig. 3. The results demonstrate that entanglement effects can stably enhance model performance. This indicates that the advantages in nonlinear fitting task introduced by entanglement effects are generalizable.

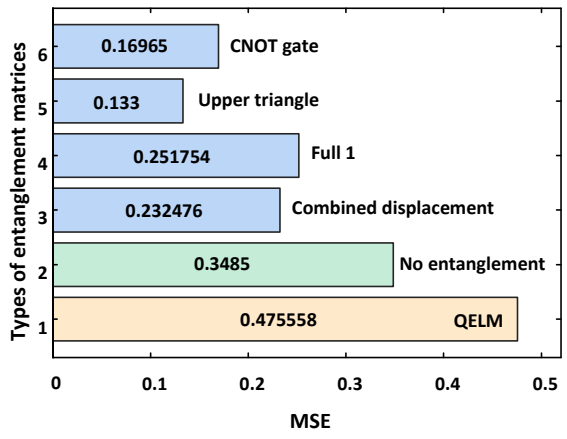

Fig. 3. Fitting error of Two-Dimensional Quantum Walk Reservoir Computing with different entanglement coins, no entanglement coins and Quantum Extreme Learning Machine

B. Abalone age prediction task

In this prediction task, the length and diameter features from the Abalone data set are used as input variables for predicting the abalone's age, i.e., number of rings. To ensure consistency in parameter numbers, the QELM model encodes length and diameter into two degrees of freedom of the input polarization state and performs six steps of quantum walk. In contrast, the 2D-QWRC model encodes the same features by two walkers respectively and performs two steps of quantum walk.

The data set is divided into training and testing subsets. The maximum tolerance error is set to 0.1. As shown in Fig. 4, the QELM model attain an accuracy of 81.35%, while the 2D-QWRC model achieved 82%. These results validate the efficacy of the 2D-QWRC model in addressing general machine learning prediction tasks. It indicates the prediction performance has reached the level of state-of-the-art quantum models such as the QELM in the literature.

However, the experiments in this paper also demonstrate that introducing an entanglement coin operator into the prediction task did not significantly enhance prediction accuracy. Furthermore, since entanglement effects are represented by a linear operator in this study, the performance improvement observed in nonlinear regression tasks is likely attributable to a redistribution of system entanglement entropy within the system. This entropy redistribution may also explain the varying degrees of optimization achieved with different coin operators. Consequently, to further exploit the impact of quantum entanglement on 2D-QWRC performance, investigating the complex entanglement dynamics within this quantum system and adopting more precise physical models are both valuable future research directions.

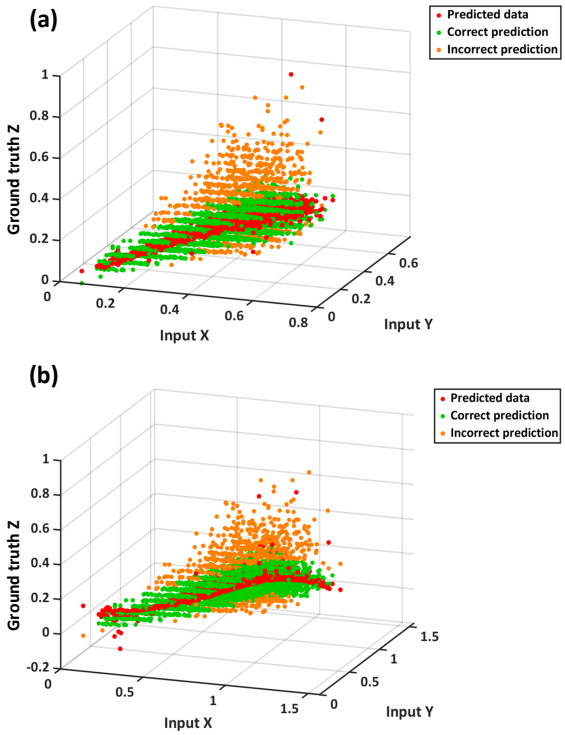

Fig. 4. Abalone age prediction task performance with (a) Quantum extreme learning machine and (b) Two-dimensional quantum walk reservoir computing.

IV. CONCLUSION

This paper presents an optical two-dimensional quantum walk reservoir computing model that aims to address the issue

of insufficient nonlinear fitting capability in advanced quantum computing such as the quantum extreme learning machine model. This study demonstrates a 64.32% improvement over the quantum extreme learning machine model in nonlinear function approximation tasks. Furthermore, the effectiveness in general machine learning tasks of the two-dimensional quantum walk reservoir computing model has been validated through the abalone age prediction task, providing a promising solution for optical quantum computing applications.

REFERENCES

[1] M. Yan et al., "Emerging opportunities and challenges for the future of reservoir computing," Nature Communications, vol. 15, no. 1, pp. 2056, Mar. 2024, doi: 10.1038/s41467-024-45187-1.

[2] J. Dudas et al., "Quantum reservoir computing implementation on coherently coupled quantum oscillators," npj Quantum Information, vol. 9, no. 1, pp. 64, Jul. 2023, doi: 10.1038/s41534-023-00734-4.

[3] L. Wang et al., "Quantum next-generation reservoir computing and its quantum optical implementation," Physical Review A, vol. 111, no. 2, pp. 022609, Feb. 2025, doi: 10.1103/PhysRevA.111.022609.

[4] K. Nakajima et al., Reservoir Computing Theory, Physical Implementations, and Applications: Theory, Physical Implementations, and Applications. 2021. doi: 10.1007/978-981-13-1687-6.

[5] A. Senanian et al., "Microwave signal processing using an analog quantum reservoir computer," Nature Communications, vol. 15, no. 1, pp. 7490, Aug. 2024, doi: 10.1038/s41467-024-51161-8.

[6] D. Pierangeli et al., "Photonic extreme learning machine by free-space optical propagation," Photonics Research, vol. 9, no. 8, pp. 1446–1454, Aug. 2021, doi: 10.1364/PRJ.423531.

[7] A. Suprano et al., "Experimental property reconstruction in a photonic quantum extreme learning machine," Physical Review Letters, vol. 132, no. 16, pp. 160802, Apr. 2024, doi: 10.1103/PhysRevLett.132.160802.

[8] L. Innocenti et al., "Potential and limitations of quantum extreme learning machines," Communications Physics, vol. 6, no. 1, pp. 118, May 2023, doi: 10.1038/s42005-023-01233-w.

[9] A. Peruzzo et al., "Quantum walks of correlated photons," Science, vol. 329, no. 5998, pp. 1500–1503, 2010, doi: 10.1126/science.1193515.

[10] K. Kadian et al. "Quantum walk and its application domains: A systematic review" Computer Science Review, vol. 41, pp. 100419, 2021, doi: 10.1016/j.cosrev.2021.100419.

[11] T. Giordani et al., "Experimental engineering of arbitrary qudit states with discrete-time quantum walks," Physical Review Letters, vol. 122, no. 2, pp. 020503, Jan. 2019, doi: 10.1103/PhysRevLett.122.020503.

[12] W. Zhao et al., "Ultracompact silicon on-chip polarization controller," Photonics Research, vol. 12, no. 2, pp. 183–193, Feb. 2024, doi: 10.1364/PRJ.499801.

[13] X. Qiang et al., "Quantum walk computing: theory, implementation, and application," *Intelligent Computing*, vol. 3, pp. 0097, 2024, doi: 10.34133/icomputing.0097.

[14] A. Schreiber et al., "A 2D quantum walk simulation of two-particle dynamics," Science, vol. 336, no. 6077, pp. 55–58, 2012, doi: 10.1126/science.1218448.

[15] H. Tang et al., "Experimental two-dimensional quantum walk on a photonic chip," Science Advances, vol. 4, no. 5, pp. eaat3174, 2018, doi: 10.1126/sciadv.aat3174.

[16] L. Innocenti et al., "Quantum state engineering using one-dimensional discrete-time quantum walks," Physical Review A, vol. 96, no. 6, pp. 062326, Dec. 2017, doi: 10.1103/PhysRevA.96.062326.

[17] C. B. Naves et al., "Quantum walks in two dimensions: controlling directional spreading with entangling coins and tunable disordered step operator," Journal of Physics A: Mathematical and Theoretical, vol. 56, no. 12, pp. 125301, Mar. 2023, doi: 10.1088/1751-8121/acbd25.

[18] M. Veldhorst et al., "A two-qubit logic gate in silicon," Nature, vol. 526, pp. 410-414, 2015, doi: 10.1038/nature15263.